# Optically tunable guided-mode resonance filter

Dennis W. Dobbs and Brian T. Cunningham

We have demonstrated a guided-mode resonance filter (GMRF) whose properties are tunable with laser illumination through the incorporation of a nonlinear dye. Laser illumination causes a change in the refractive index of the dye-doped portion of the structure, leading to controlled tuning of the GMRF reflectance spectrum. Changes in the refractive index of dye-doped regions are proportional to the intensity of the incident laser beam and are as high as $\Delta n = 0.09$. The reflectance tuning effect occurs on a time scale of many seconds and is completely reversible upon termination of the laser illumination. 

*OCIS codes:* 050.2770, 190.4710, 230.1150, 230.4320, 260.5740.

## 1. Introduction

The nonlinear optical properties of azobenzene dyes have been extensively studied in recent years.[1–3] These materials are very attractive because large changes in the refractive index can be achieved for relatively low illumination intensities, compared to more traditional nonlinear optical materials. Azobenzene-containing polymers have been used extensively in research pertaining to all-optical switching[4–7] and optical data storage.[8–11]

It is well established that there are two primary mechanisms of refractive index change in azobenzene-containing polymers. The first mechanism is photon-induced excitation of the azobenzene molecule from the lower-energy *trans* state to the excited *cis* state. Since the *cis* isomer is bent and much more compact than the elongated *trans* isomer, increasing the fraction of *cis* state molecules will result in a net decrease in the optical density of the dye-polymer system. Therefore an increase in applied optical power results in a larger fraction of dye molecules in the excited *cis* state and thus a decrease in the refractive index of the material. The second mechanism of refractive index change in these polymers is a photoinduced birefringence caused by large-scale alignment of elongated *trans* state azobenzene molecules along the direction perpendicular to the polarization of excitation light. It is thought that *trans* state molecules that are oriented perpendicular to the electric field vector of the incident light beam do not participate in photon absorption, and thus will not be excited into the *cis* state, causing them to remain oriented perpendicular to the light polarization. However, *trans* state molecules that are excited into the *cis* state will eventually relax back to the *trans* state, with the orientation of each *trans* state molecule being effectively random upon relaxation. Thus, over a period of continuous illumination, many *cis* state molecules will randomly relax to a *trans* state that is perpendicular to the electric field, and thus be removed from the pool of excitable molecules. Eventually, a significant fraction of the azobenzene molecules will be oriented perpendicular to the electric field, leading to an increase in optical density along the direction of molecular alignment and a decrease in optical density along the direction of the electric field. Values of photoinduced birefringence as high as $\Delta n = 0.13$ have been reported[11] for amorphous azobenzene-containing polymers. For liquid crystalline polymers, values as high as $\Delta n = 0.28$ have been reported.[1] Since the photoinduced birefringence effect relies on many excitation–relaxation cycles, it is the slower of the two mechanisms of refractive index change in azobenzene-containing polymers. In addition, photoinduced birefringence is not observed in systems that do not preserve orientation, such as a dye–solvent solution.[12]

Photonic crystals have also been vigorously studied in recent years. Photonic crystal structures consist of alternating regions of high and low refractive index materials and may be characterized by a photonic

When this research was performed, the authors were with the Department of Electrical and Computer Engineering, Micro and Nanotechnology Laboratory, University of Illinois at Urbana–Champaign, 208 North Wright Street, Urbana, Illinois 61801. D. W. Dobbs (dennis.dobbs@cdm-optics.com) is now with CDM Optics, 4001 Discovery Drive, Boulder, Colorado 80303.

Received 2 February 2006; revised 17 May 2006; accepted 22 May 2006; posted 23 May 2006 (Doc. ID 67724).

0003-6935/06/287286-08$15.00/0

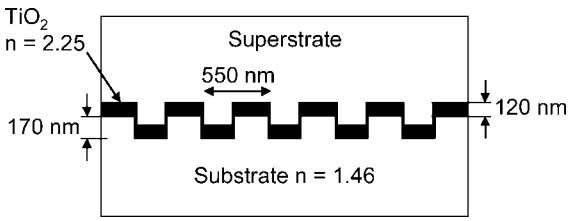

Fig. 1. Cross-sectional illustration of 1D GMRF.

bandgap. The periodic dielectric structure can lead to the formation of a photonic bandgap in much the same way that the periodic atomic potential of a semiconductor leads to the formation of electronic bandgaps.[13] Photonic crystals can be fabricated with one, two, or three dimensions of periodicity. Through careful selection of materials and structure dimensions, the optical properties of photonic crystals can be engineered for specific applications. Numerous practical applications of photonic crystals are already in widespread use, including in optical fibers,[14] tunable coupled-cavity edge-emitting semiconductor lasers,[15] vertical cavity surface emitting lasers,[16] optical biosensors,[17] and slab line-defect waveguides.[18] The most basic 1D photonic crystal, the thin-film quarter-wave stack, or distributed Bragg reflector, had been in practical use for many years before photonic crystal formalism was developed.[13] Another 1D photonic crystal, a guided-mode resonance filter (GMRF), is the structure of interest in the present work. Theoretical calculations of the spectral characteristics of GMRFs were first reported by Wang *et al*. in 1990.[19] Two years later, Magnusson and Wang[20] suggested that GMRFs could find practical application as low-loss tunable optical filters or as low-power switching elements. Additional theoretical developments concerning the use of a GMRF as an all-optical switching device were presented by Boye *et al*.[21] in 1999 and by Mizutani *et al*.[22] in 2005. There have also been investigations[23,24] into the realization of a dynamic GMRF through the use of electrical control, rather than optical control, with at least one such device having been fabricated and tested.[23]

Here we report on the fabrication and characterization of a GMRF whose reflectance spectrum is optically tunable through the incorporation of an azobenzene dye. The device, shown in Fig. 1, consists of a 1D periodic surface structure fabricated on a low refractive index plastic substrate that is overcoated with a layer of high refractive index $TiO_2$. Directly above the layer of $TiO_2$, in the superstrate region, we have applied a dye-doped polymer and a dye–solvent solution. When the fabricated structure is illuminated with broadband light at normal incidence with the light polarization perpendicular to the grating lines, a narrow band of wavelengths is strongly reflected. We have demonstrated that, upon laser illumination, the wavelength of the reflection resonance can shift to lower wavelengths by $>15$ nm and that the resonance returns to its original wavelength when the laser illumination is turned off. For the resonance tuning effect to be achieved, the wavelength of the laser must be within the absorption spectrum of the dye. We have characterized the switching speed to be of the order of many seconds. In addition, we have characterized the dependence of the magnitude of the shift on laser intensity. Because the switching behavior is largely independent of the polarization of the incident laser beam, the dominant mechanism for refractive index change is likely the *trans–cis* excitation of dye molecules in the dye-doped superstrate region. Numerical simulations show that the magnitude of the refractive index change in the dye-doped region is as large as $\Delta n = 0.09$.

### 2. Device Design and Fabrication

The GMRF, illustrated in Fig. 1, is a 1D periodic surface structure fabricated on a low refractive index plastic substrate that is overcoated with a thin film of high refractive index $TiO_2$. Directly above the $TiO_2$ film, in the superstrate region, we have applied an azobenzene dye embedded in a solid poly(methyl methacrylate) (PMMA) polymer and also in a solution of isopropyl alcohol (IPA). The dimensions of period, step height, and $TiO_2$ thickness are approximately 550, 170, and 120 nm, respectively. In addition, the sidewalls of the grating steps are covered by approximately 10 nm of $TiO_2$. The refractive indices (at a wavelength of 850 nm) of the substrate and $TiO_2$ are 1.46 and 2.25, respectively, and the refractive index of the superstrate is tunable through laser illumination. By using a nanoreplica molding process, these structures can be fabricated inexpensively on continuous rolls of flexible and transparent plastic film. A more detailed description of this fabrication process has been presented previously.[17] For this work, the plastic substrate has been adhered to a standard glass microscope slide for ease of handling.

We utilized two different superstrate materials in the present study: dye-doped PMMA and dye-doped IPA. For the dye, we chose to work with the azobenzene molecule *N*-ethyl-*N*-(2-hydroxyethyl)-4-(4-nitrophenylazo)aniline (known informally as Disperse Red 1 or DR1), since it has been thoroughly studied by many authors and is readily available (SigmaAldrich). The fabrication procedure for the samples incorporating a DR1-doped PMMA superstrate is as follows: 0.05 g of DR1 was dissolved in 3 mL of chloroform and heated to approximately 60 °C, stirring occasionally. In addition, 0.95 g of PMMA powder (SigmaAldrich, molecular weight $\approx$ 120,000) was dissolved in 8 mL of chloroform and heated to 60 °C, stirring occasionally. After both the DR1 and the PMMA had completely dissolved in their chloroform solutions, they were mixed together and stirred for 15 min. This solution was allowed to cool to room temperature, and was then spin coated onto a GMRF by using a 2000 RPM spin for 30 s. After the spin, most of the solvent had been driven off, leaving a solid film with a thickness of 1.5 μm, as measured on a surface profiler (Alpha-Step 200, Tencor). Figure 2(a) shows the absorption spectrum for this 5%

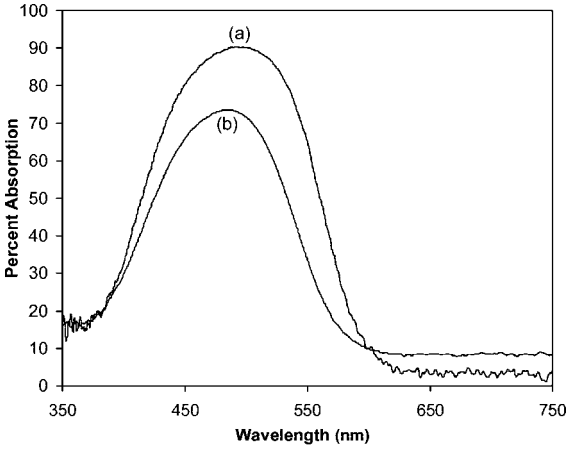


Fig. 2. (a) Absorption spectrum for 1.5-μm-thick polymer film containing 5% DR1 and 95% PMMA by weight, spun onto a blank glass microscope slide. (b) Absorption spectrum for a solution composed of 2% DR1 and 98% IPA occupying the thin layer between a microscope slide and a coverslip.

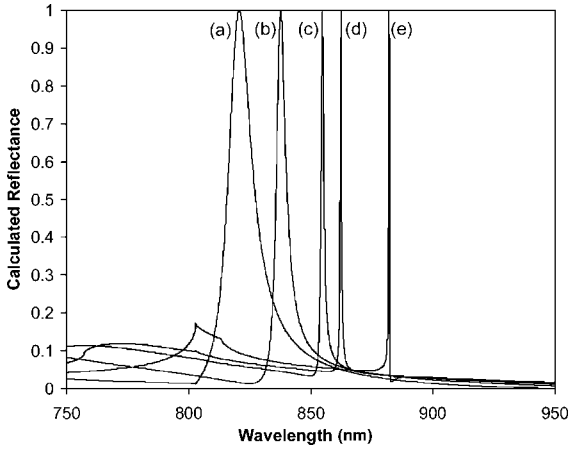


Fig. 3. Calculated normal-incidence reflectance spectra with TM polarization for five different values of the superstrate refractive index: (a) 1.00, (b) 1.20, (c) 1.333, (d) 1.377, and (e) 1.479.

DR1/95% PMMA polymer film. The wavelength of maximum absorption was measured to be 492 nm.

To construct the samples incorporating a superstrate of dye-doped IPA, 0.05 g of DR1 was dissolved in 10 mL IPA, resulting in a saturated solution. Although 0.05 g of DR1 was mixed with 10 mL of IPA, only a small amount of the DR1 dissolved in the IPA. The saturated solution of DR1 in IPA contained approximately 2% DR1 by weight. Next, a microscope coverslip was placed directly on top of the GMRF surface. A few drops of 2% DR1/98% IPA solution were placed around the edges of the coverslip, which allowed the solution to spread across the GMRF surface through capillary action. Finally, the solution was sealed underneath the coverslip by placing a bead of Duco cement around the edges of the coverslip. We estimate the depth of the 2% DR1/98% IPA solution underneath the coverslip to be 5–10 μm. The absorption spectrum for the 2% DR1/98% IPA solution is shown in Fig. 2(b). In this case, the wavelength of maximum absorption is 487 nm.

### 3. Numerical Simulations and Device Characterization

Numerical simulations of the GMRF were performed by using rigorous coupled wave analysis (RCWA). The RCWA method, first reported by Moharam and Gaylord[25] in 1981, provides a near-exact solution to Maxwell's equations for periodic diffracting structures. In this work, we utilized a commercially available implementation of the RCWA technique (DiffractMOD, RSoft Corporation).

For simulation, it was assumed that an electromagnetic plane wave is normally incident to the GMRF. The polarization of the wave was such that the electric field vector was perpendicular to the grating lines (TM polarization). To calculate a useful reflectance spectrum, the simulation was run for incident wavelengths between 750 and 950 nm, with a computation interval of 0.1 nm. A full reflection spectrum has been calculated for nine values of the superstrate refractive index. These nine values correspond to different materials that could be utilized for the superstrate. We have calculated reflectance spectra for superstrate refractive indices of 1.00, 1.333, 1.377, and 1.479, corresponding to the refractive indices of air, water, IPA, and dimethyl sulfoxide (DMSO). For instructional purposes, we have also calculated reflectance spectra for superstrate refractive indices of 1.10, 1.20, 1.30, 1.40, and 1.50, which do not necessarily correspond to actual materials. Five of these calculated reflectance spectra are shown in Fig. 3. As can be seen from Fig. 3, the predicted spectral location of the reflection peak strongly depends on the superstrate refractive index. Reflectance spectra have been measured for GMRFs with superstrates of air, water, IPA, and DMSO. Figure 4 shows a normal-incidence reflection spectrum for a GMRF with an IPA superstrate. With an IPA superstrate, the reflection peak has a FWHM of 4 nm and is located at 865.3 nm. In the figures and table, we refer to the spectral location of the reflection peak as the peak wavelength value or the PWV. Table 1 shows a comparison between the

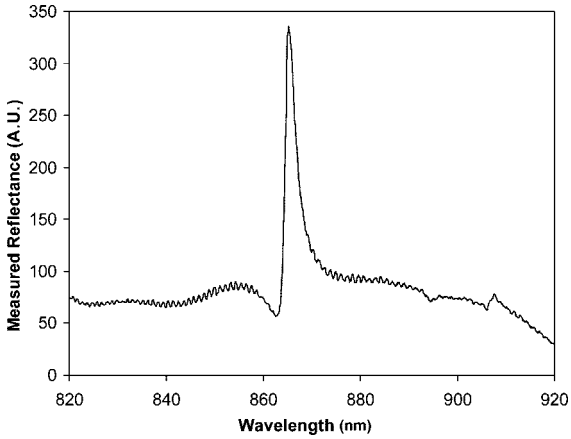


Fig. 4. Measured normal-incidence reflectance spectrum with TM polarization of a fabricated GMRF incorporating a pure IPA superstrate.

**Table 1. Measured and Calculated Peak Locations**

| Superstrate Refractive Index | Measured PWV (nm) | Calculated PWV (nm) |
|---|---|---|
| 1.000 | 820.6 | 820.7 |
| 1.333 | 856.1 | 854.8 |
| 1.377 | 865.3 | 862.4 |
| 1.479 | 881.9 | 882.1 |

calculated and the measured reflection peak locations for four different superstrate materials. The agreement between the theoretical model and the measured values is excellent, with the largest deviation being 0.3%, which occurs for the samples with an IPA superstrate. The purpose of these calculations and measurements is to develop a model of the sensitivity to refractive index changes for the GMRF. In Fig. 5, a third-order polynomial is fit to the nine calculated data points of PWV versus the superstrate refractive index. The relation between the PWV and the superstrate index for this structure is accurately approximated by the following relationship in which the PWV is in units of nanometers and $n$ is the superstrate refractive index:

$$\mathrm{PWV} = 122.07n^3 - 295.11n^2 + 290.12n + 703.61.$$

## 4. Apparatus Description

As shown in Fig. 6, we utilized a pump–probe style apparatus. A nearly collimated broadband probe beam is normally incident to the GMRF sample. Broadband light for the probe beam originated from a fiber-coupled tungsten–halogen lamp (LS-1, Ocean Optics), and a 200 μm diameter optical fiber connected the light source to a fiber collimating lens. A polarizing filter was situated between the collimating lens and the sample, so that the probe beam light was polarized perpendicularly to the grating lines of the sample. After transmission through the sample, the probe beam light was collected through a collimating lens and sent through a 200 μm diameter optical fiber to a fiber-coupled spectrometer (USB2000, Ocean Optics). A complete GMRF transmission spectrum was obtained every 20 ms during active measurement. The pump beam struck the sample at a 22.5° angle, and originated from an argon-ion laser (Innova 90, Coherent). We utilized the 488.0, 496.5, and 501.7 nm lines from the argon-ion laser, which were all strongly absorbed by DR1 molecules. The 501.7 nm line was used for illumination powers of 5 to 124 mW, the 496.5 nm line was used for illumination powers of 150 to 450 mW, and the 488.0 nm line was used for illumination powers of 500 to 1000 mW. The laser beam was not focused and had a 3 mm diameter spot size on the sample. This allowed the probe beam and pump beam to completely overlap spatially and also allowed a significant area of the GMRF surface to be utilized.

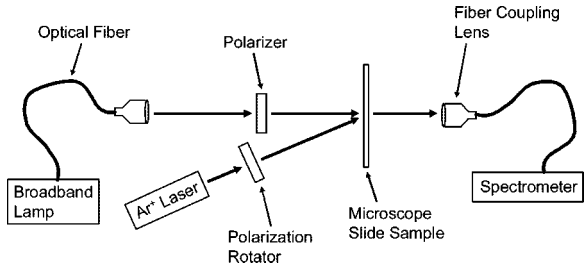


Fig. 6. Schematic showing the apparatus used to induce and measure changes in the GMRF reflection spectrum.

## 5. Results

Figures 7 and 8 show the change in the reflection peak wavelength as a function of time at three laser intensities for a GMRF coated with the 5% DR1/95% PMMA polymer film. The data presented in Fig. 7 were obtained through the use of TE-polarized laser light (laser polarization parallel to GMRF grating

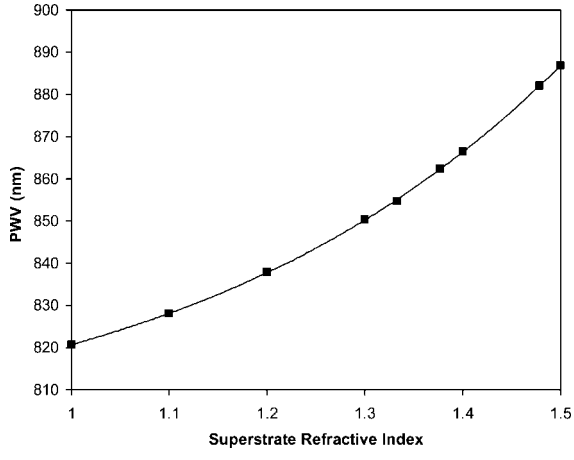


Fig. 5. Plotted points indicate the calculated spectral location of TM reflection peaks for several different superstrate material refractive indices. The continuous curve is a best-fit third-order polynomial, with $R^2 = 1$.

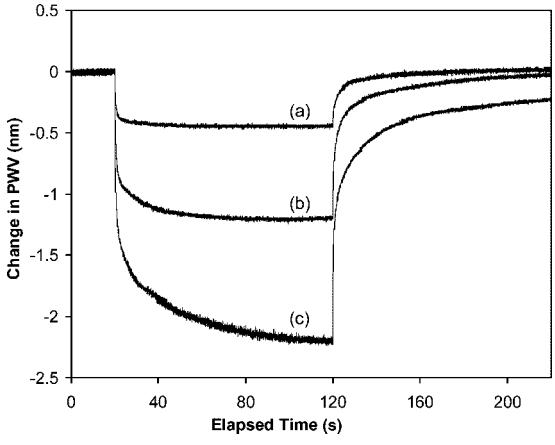


Fig. 7. Measured change in spectral location of the reflection peak of a 5% DR1/95% PMMA superstrate sample as a function of time for incident laser powers of (a) 10 mW, (b) 62 mW, and (c) 124 mW. TE-polarized laser illumination was initiated at an elapsed time of 20 s and was terminated at 120 s.

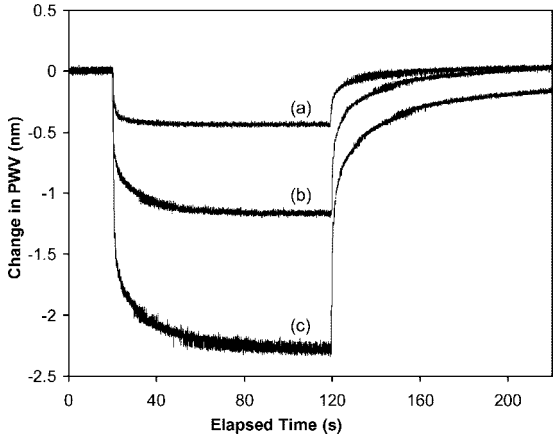


Fig. 8. Measured change in spectral location of the reflection peak of a 5% DR1/95% PMMA superstrate sample as a function of time for incident laser powers of (a) 10 mW, (b) 62 mW, and (c) 124 mW. TM-polarized laser illumination was initiated at an elapsed time of 20 s and was terminated at 120 s.

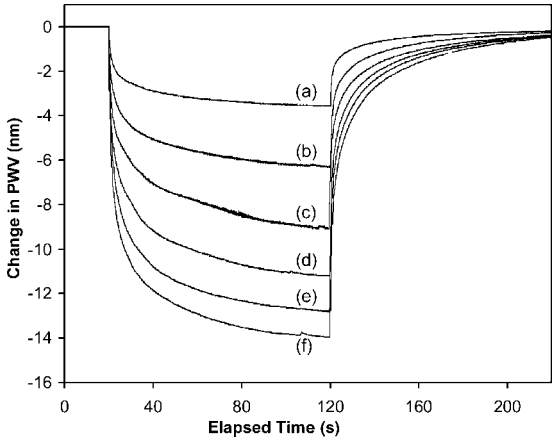


Fig. 10. Measured change in spectral location of the reflection peak as a function of time for a 2% DR1/98% IPA superstrate sample at incident laser powers of (a) 100 mW, (b) 200 mW, (c) 300 mW, (d) 400 mW, (e) 500 mW, and (f) 600 mW. TM-polarized laser illumination was initiated at an elapsed time of 20 s and was terminated at 120 s.

lines), whereas Fig. 8 is for the case of TM-polarized laser light. Laser illumination was initiated at $t = 20$ s and was terminated at $t = 120$ s. A maximum reflection peak tuning of $-2.2$ nm was achieved at the maximum laser power of 124 mW (which corresponded to an intensity of 1.75 W/cm$^2$). This magnitude of tuning corresponded to a change in the superstrate refractive index of $\Delta n \approx -0.01$, as determined from the GMRF sensitivity relationship discussed in Section 3. In Fig. 9, the maximum change in reflection peak location is plotted as a function of laser power. The square data points in Fig. 9 indicate the TE laser polarization, and the triangles indicate the TM laser polarization. Figure 9 also shows that the maximum reflection peak shift varies nearly linearly with the laser power over this range of powers. It should be noted that laser powers larger than 124 mW were not used on this sample, since the effects of photobleaching of the dye begin to become significant for powers larger than this. Photobleaching is the result of photon-induced damage to the dye molecules and is characterized by a permanent decrease in the refractive index of the dye-polymer system.

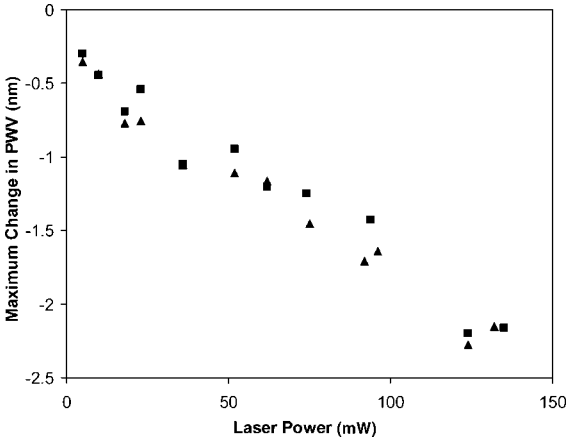


Fig. 9. Maximum change in the spectral location of the reflection peak for 5% DR1/95% PMMA superstrate samples at several values of laser illumination power. Squares indicate TE laser polarization, and triangles correspond to TM laser polarization.

In contrast, the GMRF samples that utilized the saturated solution of DR1 in IPA as the nonlinear material showed complete resistance to photobleaching. Thus we were able to perform the characterization for laser powers as high as 1000 mW (intensities as large as 14 W/cm$^2$) with no observable damage to the nonlinear material. Figure 10 shows the change in peak reflection wavelength as a function of time for several intensities of TM-polarized laser illumination. Once again, laser illumination begins at time $t = 20$ s and is terminated at time $t = 120$ s. A maximum reflection peak tuning of $-15.2$ nm was achieved at the maximum laser power of 1000 mW. This magnitude of tuning corresponds to a change in the superstrate refractive index of $\Delta n \approx -0.09$. In Fig. 11, the maximum reflection peak shift is plotted versus laser power. For laser powers between 50 and 500 mW, the relationship between maximum peak tuning and laser power is quite linear. However, for laser powers of 600 mW and higher, there appears to be some saturation of the index-change effect. In Fig. 12, the illumination-equilibrium superstrate refractive index is plotted versus laser power. This was determined by using the data of Fig. 11 in conjunction with the device sensitivity relationship described in Section 3. Figure 12 shows that the 2% DR1/98% IPA superstrate refractive index varied from approximately 1.39 when there was no laser illumination, to approximately 1.30 in the case of 1000 mW illumination.

Figure 13 illustrates the remarkable similarity between the data collected with TM- and TE-polarized incident laser light for the samples utilizing a 2% DR1/98% IPA superstrate. In Fig. 13, 200 mW of

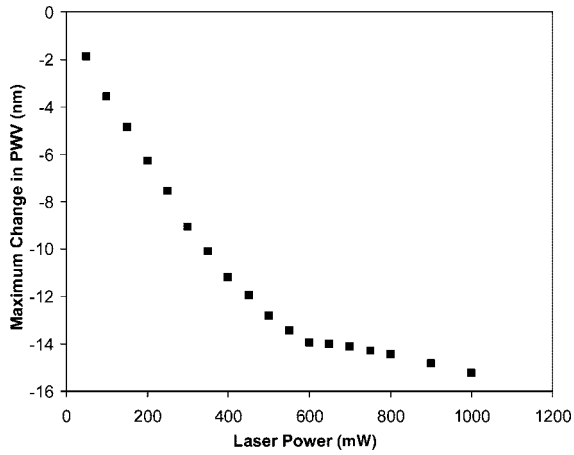


Fig. 11. Maximum change in the spectral location of the reflection peak of a 2% DR1/98% IPA superstrate sample at several intensities of TM-polarized laser illumination.

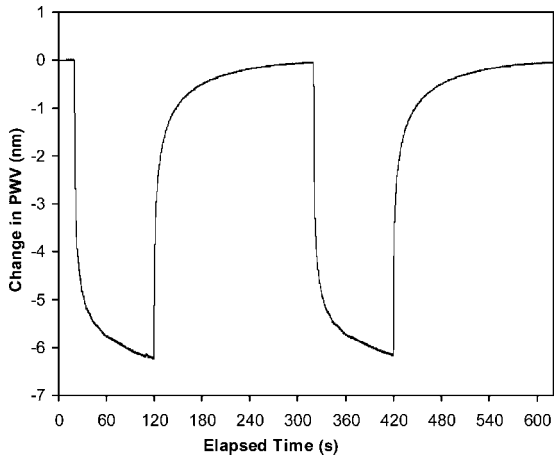


Fig. 13. Measured change in spectral location of the reflection peak as a function of time for a 2% DR1/98% IPA superstrate sample at an incident laser power of 200 mW. TM-polarized laser illumination was initiated at an elapsed time of 20 s and was terminated at 120 s. TE-polarized laser illumination was initiated at an elapsed time of 320 s and was terminated at 420 s.

TM-polarized laser illumination is initiated at $t = 20$ s and is terminated at $t = 120$ s. Within the time that the laser beam is blocked (between $t = 120$ s and $t = 320$ s), the polarization of the laser beam is rotated by 90°. Then, at $t = 320$ s, the beam is unblocked, and the GMRF is illuminated with 200 mW of TE-polarized laser light. Laser illumination is terminated at $t = 420$ s. As can be seen in Fig. 13, the magnitude of peak shifting and the transient response is nearly identical between these two cases of laser polarization.

## 6. Discussion

For the samples utilizing a 5% DR1/95% PMMA superstrate, it is clear that the tuning behavior for the case of TE laser polarization (Fig. 7) is very similar to the case of TM laser polarization (Fig. 8). This suggests that the dominant mechanism of refractive index change is the *trans–cis* excitation, rather than photoinduced birefringence. At the onset of laser illumination, many *trans* isomer dye molecules in the polymer film are excited to the *cis* isomer state, causing a decrease in the refractive index in the polymer film, and thus leading to a shift toward smaller wavelengths in the spectral location of the GMRF reflection peak. Then, upon the termination of laser illumination, the excited state *cis* isomers undergo thermal relaxation back to the *trans* isomer state, causing the refractive index of the polymer film to return to its initial value, and thus the reflection peak wavelength returns to its initial value. In contrast, if photoinduced birefringence were the dominant mechanism of refractive index change, then we would expect significant differences in tuning behavior between the two laser polarizations. Indeed, for other dye-polymer systems, we have observed the reflection peak wavelength increase when laser polarization is parallel to the grating lines (TE polarization), with a decrease for the case of laser polarization perpendicular to the grating lines (these data not shown). However, it should be noted that upon careful inspection, minor differences between Figs. 7(c) and 8(c) are evident, particularly in the transition rate. In Fig. 7(c), for the case of TE laser polarization, the downward transition is more gradual than the downward transition in Fig. 8(c). It is possible that this difference can be explained by the presence of a small amount of photoinduced birefringence. TM-polarized laser light should cause some of the dye molecules to become oriented parallel to the grating lines, which would reinforce the tendency for the reflection peak location to shift downward in wavelength. Conversely, TE-polarized laser light should cause some of the dye molecules to become oriented perpendicularly to the grating lines, which would provide a tendency toward an upward shift in the reflection peak wavelength. In this case, however, photoinduced birefringence is a minor effect, and thus, for the case of TE laser polarization, photoinduced birefringence merely acts to

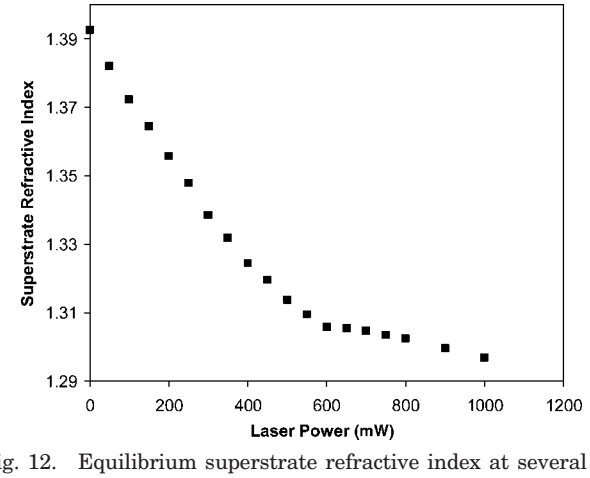


Fig. 12. Equilibrium superstrate refractive index at several intensities of TM-polarized laser illumination, as determined from the measured data of Fig. 11 in conjunction with the device sensitivity relationship discussed in Section 3.

slightly counteract the tendency toward a downward shift in reflection peak wavelength. For the case of TM laser polarization, photoinduced birefringence acts to slightly reinforce the tendency toward a downward shift in the spectral location of the reflection peak.

Upon comparing Figs. 7 and 8 with Fig. 10, it is clear that the tuning behavior for the 5% DR1/95% PMMA superstrate samples is very similar to that of the 2% DR1/98% IPA superstrate samples. In addition, for the 2% DR1/98% IPA superstrate samples we observed that the reflection peak tuning behavior for the TM-polarized laser illumination was nearly identical to the tuning behavior for the TE-polarized laser illumination, as can be seen from the data presented in Fig. 13. Thus we conclude that the dominant mechanism of refractive index change in the 2% DR1/98% IPA superstrate samples is the *trans–cis* excitation of dye molecules. This is certainly to be expected as the liquid solvent does not allow for long-term alignment of the *trans*-state dye molecules. In low-viscosity solutions such as IPA, small molecules are known to diffuse rotationally within a few picoseconds.[12] Thus there is not any appreciable photoinduced birefringence, and one can be quite certain that the refractive index change is caused by the *trans–cis* excitation.

As mentioned previously, Fig. 11 shows that there is some saturation of the index-change effect for laser powers of 600 mW and greater for the samples utilizing a 2% DR1/98% IPA superstrate. For laser powers larger than 600 mW, further increases in illumination power do not yield significant additional shifting of the reflection peak. We interpret this to mean that most of the available dye molecules are in the excited *cis* state at an illumination power of 600 mW. Although there appears to be an obvious saturation point at 600 mW, a careful inspection of Fig. 11 shows that there is still a small amount of additional shifting as the laser power is further increased. For illumination powers greater than the 600 mW saturation point, it is possible that the small amounts of observed additional shifting are caused by the heating of the sample.

An inspection of Figs. 7, 8, 10, and 13 reveals that the tuning response time is of the order of many seconds, and that it takes longer than 1 min for the spectral location of the reflection peak to reach its equilibrium position. Although the response time demonstrated here is slower than that required for many optical switching applications, this device concept could be used with a faster nonlinear material. In particular, the simple, low-cost nanoreplica molding fabrication process utilized here allows for the choice of a wide variety of nonlinear superstrate materials. In addition, GMRFs allow for easy determination of the refractive index of superstrate material, which could be useful in characterization of the nonlinear material itself.

## 7. Conclusion

We have demonstrated 1D GMRF whose reflectance spectrum is tunable with laser illumination through the incorporation of a nonlinear azobenzene dye. Laser illumination causes a change in the refractive index of the dye-doped region of the structure, leading to controlled tuning of the GMRF reflectance spectrum. The spectral location of the primary reflection feature was shifted by >15 nm, and the shift was completely reversible upon termination of the laser illumination. Numerical simulations show that this level of tuning corresponds to a refractive index change of $\Delta n = 0.09$ in the dye-doped region. We anticipate that tunable GMRFs will have applications in optical switching, laser modulation, and as tools for nonlinear optical material research.

This research was supported by the U.S. Army Soldier Systems Center (Brian R. Kimball) under the auspices of the U.S. Army Research Office Scientific Services Program administered by Battelle (Delivery Order 0505, contract DAAD19-02-D-0001). The experimental portion of this work was carried out in the Laser and Spectroscopy Facility of the Frederick Seitz Materials Research Laboratory, University of Illinois, which is partially supported by the U.S. Department of Energy under grant DEFG02-91-ER45439. The authors thank Julio A. Soares for his facilitation of the use of the Laser and Spectroscopy Facility.

## References

1. F. J. Rodriguez, C. Sanchez, B. Villacampa, R. Alcala, R. Cases, M. Millaruelo, and L. Oriol, "Optical anisotropy and nonlinear optical properties of azobenzene methacrylic polymers," Polymer **45,** 2341–2348 (2004).
2. Y. J. Wang and G. O. Carlisle, "Optical properties of disperse-red-1-doped nematic liquid crystal," J. Mater. Sci.: Mater. Electron. **13,** 173–178 (2002).
3. Y. W. Yi, T. E. Furtak, M. J. Farrow, and D. M. Walba, "Photoinduced anisotropy of second-harmonic generation from azobenzene-modified alkylsiloxane monolayers," J. Vac. Sci. Technol. A **21,** 1770–1775 (2003).
4. M. Ivanov, D. Ilieva, G. Minchev, T. Petrova, V. Dragostinova, T. Todorov, and L. Nikolova, "Temperature-dependent light intensity controlled optical switching in azobenzene polymers," Appl. Phys. Lett. **86,** 181902 (2005).
5. H. Wang, Y. Huang, Z. Liu, F. Zhao, W. Lin, J. Wang, and Z. Liang, "Ultrafast photoinduced anisotropy and optical switching in azobenzene sidechain polymers," Appl. Phys. Lett. **82,** 3394–3396 (2003).
6. S. Wu, S. Luo, W. She, D. Luo, and H. Wang, "All-optical switching effects in poly(methyl methacrylate) composites," React. Funct. Polym. **56,** 83–88 (2003).
7. Y. Luo, W. She, S. Wu, F. Zeng, and S. Yao, "Improvement of all-optical switching effect based on azobenzene-containing polymer films," Appl. Phys. B **80,** 77–80 (2005).
8. T. G. Pedersen, P. M. Johansen, and H. C. Pedersen, "Characterization of azobenzene chromophores for reversible optical data storage: molecular quantum calculations," J. Opt. A **2,** 272–278 (2000).
9. P. Wu, D. V. G. L. N. Rao, B. R. Kimball, M. Nakashima, and B. S. DeCristofano, "Nonvolatile grating in an azobenzene polymer with optimized molecular reorientation," Appl. Phys. Lett. **78,** 1189–1191 (2001).
10. Y. Aoshima, C. Egami, Y. Kawata, O. Sugihara, M. Tsuchimori, O. Watanabe, H. Fujimura, and N. Okomoto, "The optical properties of azobenzene-containing urethane-urea copolymer films for data storage," Polym. Adv. Technol. **11,** 575–578 (2000).

11. L. L. Nedelchev, A. S. Matharu, S. Hvilsted, and P. S. Ramanujam, "Photoinduced anisotropy in a family of amorphous azobenzene polyesters for optical storage," Appl. Opt. **42,** 5918–5927 (2003).
12. Z. Sekkat, "Photo-orientation by photoisomerization," in *Photoreactive Organic Thin Films,* Z. Sekkat and W. Knoll, eds. (Academic, 2002), pp. 63–104.
13. J. D. Joannopoulos, R. D. Meade, and J. N. Winn, *Photonic Crystals* (Princeton U. Press, 1995).
14. P. Russell, "Photonic crystal fibers," Science **299,** 358–362 (2003).
15. S. Mahnkopf, R. Marz, M. Kamp, G. Duan, F. Lelarge, and A. Forchel, "Tunable photonic crystal coupled-cavity laser," IEEE J. Quantum Electron. **40,** 1306–1314 (2004).
16. N. Yokouchi, A. J. Danner, and K. D. Choquette, "Two-dimensional photonic crystal confined vertical-cavity surface-emitting lasers," IEEE J. Sel. Top. Quantum Electron. **9,** 1439–1445 (2003).
17. B. Cunningham, B. Lin, J. Qiu, P. Li, J. Pepper, and B. Hugh, "A plastic colorimetric resonant optical biosensor for multiparallel detection of label-free biochemical interactions," Sens. Actuators B **85,** 219–226 (2002).
18. M. Tokushima and H. Yamada, "Light propagation in a photonic-crystal-slab line-defect waveguide," IEEE J. Quantum Electron. **38,** 753–759 (2002).
19. S. S. Wang, R. Magnusson, J. S. Bagby, and M. G. Moharam, "Guided-mode resonances in planar dielectric-layer diffraction gratings," J. Opt. Soc. Am. A **7,** 1470–1474 (1990).
20. R. Magnusson and S. S. Wang, "New principle for optical filters," Appl. Phys. Lett. **61,** 1022–1024 (1992).
21. R. R. Boye, R. W. Ziolkowski, and R. K. Kostuk, "Resonant waveguide-grating switching device with nonlinear optical material," Appl. Opt. **38,** 5181–5185 (1999).
22. A. Mizutani, H. Kikuta, and K. Iwata, "Numerical study on an asymmetric guided-mode resonant grating with a Kerr medium for optical switching," J. Opt. Soc. Am. A **22,** 355–360 (2005).
23. A. Sharon, D. Rosenblatt, A. A. Friesem, H. G. Weber, H. Engel, and R. Steingrueber, "Light modulation with resonant grating-waveguide structures," Opt. Lett. **21,** 1564–1566 (1996).
24. H. Ichikawa and H. Kikuta, "Dynamic guided-mode resonant grating filter with quadratic electro-optic effect," J. Opt. Soc. Am. A **22,** 1311–1318 (2005).
25. M. G. Moharam and T. K. Gaylord, "Rigorous coupled-wave analysis of planar-grating diffraction," J. Opt. Soc. Am. **71,** 811–818 (1981).